Land Degradation & Development

WILEY

RESEARCH ARTICLE OPEN ACCESS

Evaluation of Sediment Connectivity Indices to Improve the Prediction of the Spatiotemporal Variability of Sediment Yield for a Large River Basin (Wei River, China)

Zhenni Wu[1] | Jantiene E. M. Baartman[1] | João Pedro Nunes[1] | Manuel López-Vicente[2]

[1]Soil Physics and Land Management Group, Wageningen University, Wageningen, the Netherlands | [2]GEOFOREST, Departamento de Ciencias Agrarias y del Medio Natural, Escuela Politécnica Superior de Huesca, Instituto de Investigación en Ciencias Ambientales (IUCA), Universidad de Zaragoza, Huesca, Spain

Correspondence: Zhenni Wu (zhenni.wu@wur.nl)

Received: 3 September 2024 | **Revised:** 12 May 2025 | **Accepted:** 16 November 2025

Keywords: aggregated index of connectivity | large basin | sediment connectivity | sediment yield | temporal variability

ABSTRACT

Sediment connectivity between source areas and the main streams or local sinks is a complex and dynamic process, especially in large basins due to multiple heterogeneities and interactions between connectivity components. Sediment connectivity indices are promising tools to investigate sediment transport, especially in data-scarce or large areas. The InVEST-SDR numerical approach couples RUSLE gross erosion estimates with the Index of Connectivity (IC) to derive sediment delivery. However, involving functional connectivity and validating the results remains challenging. In a first estimate, we used the coupled InVEST-SDR approach to calculate the annual sediment yield in the entire Wei River Basin (134,800 km^2) and three of its sub-catchments. Then, we replaced the IC with the Aggregated Index of Connectivity (AIC), which includes functional connectivity aspects. Computational results were compared with observation data from 26 hydrometric stations to verify the performance of the simulations. Both IC and AIC performed well in predicting sediment yield, with $R^2 > 0.91$. The areas with the highest connectivity (90th percentile—P90) also showed high values of erosion: 54% of the P90 values were found in the three catchments with the highest observed sediment yield. The rainfall erosivity and soil permeability factors were found to be the main explanatory components of the difference in spatial domination of structural (no temporary changes) and functional (temporally dynamic) connectivity. This study demonstrated the accuracy of AIC for sediment transport and yield evaluation in a large river basin. This method is potentially beneficial for land management in large basin areas with insufficient data.

1 | Introduction

Sediment transport can lead to significant adverse effects, including the depletion of soil fertility in agricultural areas, contamination of water bodies, obstruction of reservoirs, alteration of riverbeds, and an increased risk of flooding (Wohl 2015). These consequences can collectively result in substantial economic losses (Vázquez-Tarrío et al. 2024). In small and medium-sized basins, prediction models of sediment yield offer accurate estimates. However, in large basins (> 10,000 km^2), models only provide reliable results where the considered processes are indeed dominant, and model accuracy requires more input data and higher calibration efforts (de Vente et al. 2013). In the last two decades, sediment connectivity has become an emerging concept to analyze and manage sediment transport in catchments (Marchi et al. 2019; Zanandrea et al. 2021). Sediment connectivity describes the potential of sediment transfer from source to sink areas through the watershed, and emphasizes the extent of linkage of different compartments of the system, such as slopes and river streams (Najafi et al. 2021). Furthermore, sediment connectivity varies in response to human activities, such as land use change, and urbanization and construction of soil and water conservation measures (Llena et al. 2019; Persichillo et al. 2018; Poeppl et al. 2017). Two concepts derived from connectivity are structural connectivity and functional connectivity, where structural connectivity indicates the physical linkage of the landscape (without considering temporal changes in the evaluated parameters) while functional connectivity is related to process-based sediment transport processes in different components of the system (Bracken et al. 2015).

Various connectivity indices have been developed and applied to quantify the degree of connection between sources and sinks of sediment. One of the earliest and most widely used is the Index of Connectivity (IC), developed by Borselli et al. (2008). This index uses a computer-based GIS (Geographic Information System) approach to calculate the potential connectivity between downslope and upslope components, taking into account catchment area, distance from source to sink, slope angle and the role of vegetation cover as a sediment transport impedance factor. Cavalli et al. (2013) then modified and extended this index to suit mountain areas by introducing the Manning's n roughness into the weight factor, and developed a free open-source tool, SedInConnect, which made this index widely applied (Crema and Cavalli 2018). Most modelling approaches and indices involve structural elements rather than functional in current research (Najafi et al. 2021). However, variants of connectivity indices are being developed based on IC that incorporate functional features (Bombino et al. 2020; Cislaghi and Bischetti 2019; Persichillo et al. 2018; Zingaro et al. 2019). For example, Bombino et al. (2020) included a flow conditions factor which takes rainfall and infiltration into account; Zingaro et al. (2019) involved annual average rainfall. The Aggregated Index of sediment Connectivity (AIC) developed by López-Vicente and Ben-Salem (2019) is another derivative of the IC; it incorporates as weight factors both static variables such as soil permeability and roughness of the terrain, and dynamic variables such as rainfall erosivity.

Connectivity indices are relatively easy to calculate, as compared to for example process-based erosion models (Najafi et al. 2021). However, the challenges of assessing the modelling results of connectivity remain, especially in large basins, since in terms of connectivity every pathway needs to be followed to identify potential disconnections (Hooke and Souza 2021). One possible approach is to assess its effects on the Sediment Delivery Ratio (SDR), (de Vente et al. 2016). Vigiak et al. (2012) developed the Integrated Valuation of Ecosystem Services and Tradeoffs (InVEST) SDR model which computes SDR from IC using an empirical equation. The combined use of IC and a soil erosion model (e.g., revised MMF) can be a suitable approach to derive maps of sediment trap effectiveness across the landscape (López-Vicente et al. 2013). Several studies used the InVEST-SDR model to estimate sediment export at the watershed scale (Abebe et al. 2023; Bhattacharya et al. 2024; Gashaw et al. 2021), but the model has not been tested in large basins, which is of practical importance for local soil and water management. Furthermore, this model has not been coupled with functional connectivity to examine the possibility of functional connectivity in sediment yield prediction.

The implementation of connectivity in designing sediment management measures is especially important in developing and newly industrialized countries, where severe soil erosion and loss takes place and causes serious economic impacts, while long-term and high-resolution observation data are insufficiently available for analysis with for example process-based models (Didoné et al. 2017; Mekonnen et al. 2016; Najafi et al. 2021). For instance, Tangi et al. (2023) optimized reservoir sediment management strategies to maximize hydropower generation on the lower Mekong River using connectivity. The Chinese Loess Plateau consists of about 300 m of highly erodible loess deposits (Zhu et al. 2019), experiences intense summer rainfall and reduced vegetation due to human disturbance, resulting in severe soil erosion that contributes approximately 90% of the sediment load to the Yellow River (Tian et al. 2023). At the large river basin scale, such as the Wei River Basin (134,800 km^2) in the Loess Plateau, it is useful to simulate the uneven spatial distribution of sediment flux variation in terms of morphology variations (Delmas et al. 2009). To restore the fragile ecosystems in the Loess Plateau, the Chinese government has implemented the 'Grain for Green Project' since 1999, in which large areas of sloping farmland have been converted into forest and grassland, and the vegetation coverage has significantly increased within 10 years (Zhao et al. 2013), thus the Loess Plateau provides an ideal platform for sediment connectivity research.

This study aimed to assess the performance of two sediment connectivity indices –the IC and AIC approaches– for predicting sediment yield across a large basin using the InVEST-SDR model. In particular, we: (1) validated the sediment connectivity result using observed sediment discharge data of 26 hydrometric stations in the Wei River Basin from 2001 to 2011; (2) evaluated the spatial and temporal variations of sediment connectivity in the 11 years after the large-scale ecological restoration project that was launched in the Wei River Basin; and (3) identified the structural and functional connectivity dominant areas. The findings of this study are relevant for informing soil conservation measures and mitigating sediment export to rivers and reservoirs.

2 | Materials and Methods

2.1 | Study Area

The Wei River (Figure 1) is the largest tributary of the Yellow River. It originates from Niaoshu Mountain, runs through the provinces of Gansu, Ningxia, and Shaanxi, and merges into the Yellow River at Tongguan County. The Wei River has two main tributaries in the basin, the Jing River and the Beiluo River. The basin is located in central China and has a drainage area of 134,800 km^2. The northern part of the basin is located in the Loess Plateau and the southern part belongs to the Qinling Mountains. The whole basin includes three sub-catchments: Wei sub-catchment (the west and south branch); Jing sub-catchment (the middle branch); Beiluo sub-catchment (the east branch). The Wei River Basin is located in a semi-arid continental climate area, with a mean annual precipitation ranging between 381 and 860 mm that is concentrated in summer. The mean annual rainfall erosivity in the basin ranges from 751 to 2600 MJ mm hm^{-2} h^{-1}, and the mean annual air temperature ranges from 7.8°C to 13.5°C (Zhang et al. 2021). A considerable area of the basin is covered by thick loess deposits, which

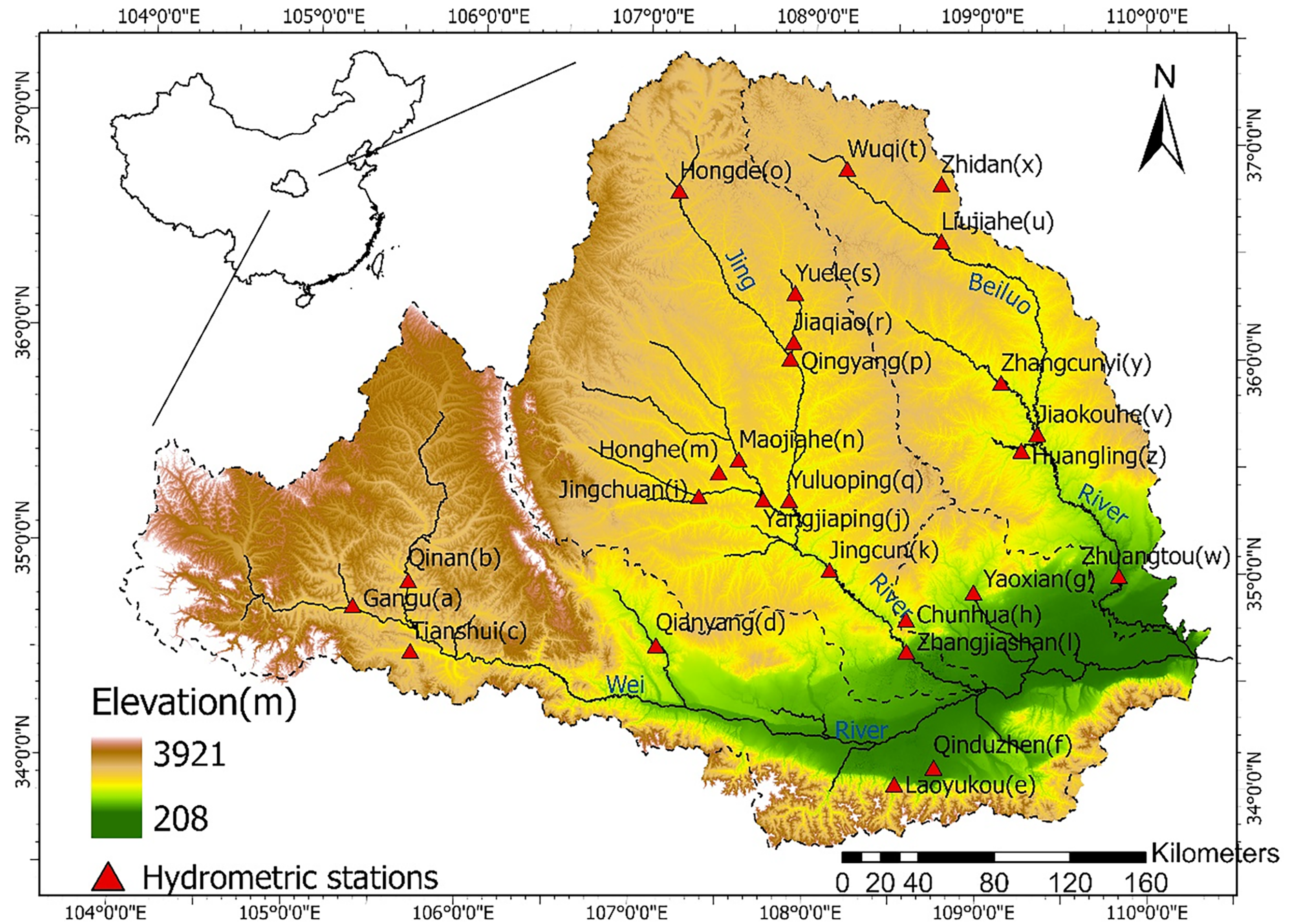

FIGURE 1 | Location and elevation of the study area and the selected hydrometric stations. [Colour figure can be viewed at wileyonlinelibrary.com]

are porous and relatively loose with good permeability but poor erosion resistance (Liu et al. 2022). The dominant land uses are farmland (wheat and maize) and grassland, which cover 40.5% and 38.2%, respectively.

2.2 | Estimation of Soil Erosion Using RUSLE Model

The annual soil loss rate due to water erosion (E; t year^{-1}) was estimated using the RUSLE empirical equation, which is expressed as follows:

$$E = R \times K \times \mathrm{LS} \times C \times P \times A \tag{1}$$

where R is the rainfall erosivity factor (MJ mm ha^{-1} h^{-1} year^{-1}), K is the soil erodibility factor (t hm^2 h MJ^{-1} mm^{-1} hm^{-2}), LS is the slope length-steepness factor, C is the land cover and management factor (values between 0 and 1), P is the support practices factor (values between 0 and 1), and A is the area of research (ha). The LS, C and P factors are dimensionless.

The R factor was calculated from the method described in (Xie et al. 2016):

$$R_{\mathrm{day}} = \alpha {P_d}^{1.7265} \quad (P_d > 10\ \mathrm{mm}) \tag{2}$$

where R_{day} is the daily rainfall erosivity, P_d is the daily rainfall amount (including only > 10 mm rainfall), α is the seasonal coefficient (0.3101 from May to September, 0.3937 from October to April). Then, the annual rainfall erosivity was accumulated from the daily rainfall erosivity.

The K factor was downloaded from the repository of the European Soil Data Centre (ESDAC), based on the study made by Borrelli et al. (2017). The S factor was computed using an equation developed by B. Liu et al. (1994), which includes > 18% slopes that are widespread on the Loess Plateau (Equation 3), and the L factor was calculated using the method developed through field measurements mainly from the Loess Plateau (Li, Guan, et al. 2022).

$$S = \begin{cases} 10.8 \sin\theta + 0.03, & 9\% > \theta > 0 \\ 16.8 \sin\theta - 0.5, & 18\% \geq \theta \geq 9\% \\ 21.91 \sin\theta - 0.96, & \theta > 18\% \end{cases} \tag{3}$$

$$L = \left(\frac{\gamma}{22.13}\right)^m \begin{cases} m = 0.45, & m \geq 40\% \\ m = 0.35, & 40\% > m \geq 21\% \\ m = 0.2, & 21\% > m \geq 9\% \\ m = 0.15, & 9\% > m \geq 0 \end{cases} \tag{4}$$

The C factor was estimated from the ground cover maps provided by (Yang et al. 2020) and using their method:

$$\mathrm{SLR}_i = e^{-0.0418(\mathrm{TC}_i - 5)} \tag{5}$$

$$C_i = \mathrm{SLR}_i \times \mathrm{EI}_i / \mathrm{EI}_t \tag{6}$$

$$C = \sum_{i=1}^{12} C_i \tag{7}$$

where SLR_i is the soil loss ratio in month i, TC_i is the total percentage of ground cover, C_i is the monthly C factor in month i, EI_i and EI_t are the monthly and yearly rainfall erosivity respectively.

The P factor was calculated from land use data in 2015 and the assigned values in previous studies on the Loess Plateau (Li, Chen, et al. 2022), where forest, grassland, marsh, farmland with a slope less than 2% and bare land are 1, waterbody and construction land are 0. The p value for farmland with a slope greater than 2% was calculated using the method proposed by (Lufafa et al. 2003):

$$P = 0.2 + 0.03s \tag{8}$$

where s (%) represents the slope gradient; terraces were not taken into consideration here.

2.3 | Computation of Sediment Connectivity

In this study, we calculated sediment connectivity using the Index of sediment Connectivity (IC) developed by Borselli et al. (2008) for the structural connectivity assessment, and the AIC proposed by López-Vicente and Ben-Salem (2019) for the functional connectivity assessment. The method for calculating the IC is detailed in the work by Borselli et al. (2008). AIC considers the spatial heterogeneity of rainfall, land uses, topography and soil physical properties through five factors:

$$\mathrm{AIC}_k = \log_{10}\left(\frac{D_{\mathrm{UP},K}}{D_{dn,k}}\right) = \log_{10}\left(\frac{\overline{R_t} \cdot \overline{\mathrm{RT}} \cdot \overline{C_t} \cdot \overline{K_P} \cdot \overline{S} \cdot \sqrt{A_K}}{\sum_{k=i}^{n} \frac{d_i}{\mathrm{AWC}_i}}\right) \tag{9}$$

$$\mathrm{AWC}_i = R_{ti} \cdot \mathrm{RT}_i \cdot C_{ti} \cdot K_{pi} \cdot S_i \tag{10}$$

where AWC is the aggregated weighting factor. R_t is the rainfall erosivity factor of the period t, C_t is the vegetation and crop management factor of the period t; both C and R factors were calculated using the same method as the RUSLE equations (Equations 2 and 7). RT is the roughness of the terrain factor, which was calculated as the inverse values of the standard deviation of the normalized slope gradient. K_p is the soil permeability factor, which was computed from the normalized and inverse values of available soil water. Values of RT and K_p were inversed because higher surface roughness and soil permeability induce lower overland flow velocity and magnitude, respectively, and thus lower sediment connectivity. S is the slope gradient factor ($\mathrm{m\,m^{-1}}$), which was calculated using the slope gradient tool in ArcGIS Pro. All factors were normalized into values between 0.001 and 1. In this study, the computation target was the river network. The maps of sediment connectivity were generated by running the algorithm procedure in the updated Borselli's index (Borselli et al. 2008) and combining the AIC weighting factors. Yearly AIC map were calculated with yearly C factor and R factor maps. More details about input parameters and index setup can be found in (López-Vicente and Ben-Salem 2019; Wu et al. 2023).

2.4 | Estimation of Sediment Yield

The InVEST-SDR model (Hamel et al. 2015) was applied in this study to estimate sediment yield. First, the SDR for each pixel i is derived from the original IC connectivity index (Vigiak et al. 2012):

$$\mathrm{SDR}_i = \frac{\mathrm{SDR}_{\mathrm{Max}}}{1 + \exp\left(\frac{\mathrm{IC}_0 - \mathrm{IC}_i}{k_b}\right)} \tag{11}$$

where $\mathrm{SDR}_{\mathrm{Max}}$ is the maximum theoretical SDR, which is set to a default value of 0.8 based on the InVEST-SDR model user guide. This value is consistent with the findings of Tian et al. (2022), who suggest that SDRs in the Wei River Basin are generally expected to be lower than 1.0. Besides, Lu et al. (2006) found in the Australian Murray Darling Basin ($1.1 \times 10^6\,\mathrm{km}^2$, about 14% of Australia), which has a comparable size to our study area, that the catchment sediment residence time is a key factor controlling the sediment delivery process, with SDR values from close to 0 in floodplains to 0.70 in the eastern uplands of the Basin IC_0 and k_b are calibration parameters that define the shape of the SDR-IC relationship. In this study, we applied $\mathrm{IC}_0 = 0.5$ and $k_b = 2$ for a linear shape.

The estimated sediment yield from each pixel i, ESY_i ($\mathrm{t\,year^{-1}}$), was calculated as a function of the RUSLE estimated soil loss E_i (see Equation 1) and SDR factor, representing the amount of sediment eroded from a certain pixel and that reaches the stream:

$$\mathrm{ESY}_i = E_i \times \mathrm{SDR}_i \tag{12}$$

The total catchment estimated sediment yield or export (ESY; t $\mathrm{year^{-1}}$) is given by:

$$\mathrm{ESY} = \sum i\mathrm{ESY}_i \tag{13}$$

The ESY was evaluated using both the original IC, but also using the AIC. This study represents the first attempt to integrate the InVEST-SDR model with functional connectivity.

2.5 | Model Verification

The yearly sediment yield (SY) data from 26 hydrological stations located in the study area (Figure 1) were used to verify the model performance. These data were extracted from the China Water Resources Bulletin (Ministry of Water Resources); the consistency and reliability of the data were checked by the Ministry of Water Resources before data release. These data were recorded on a daily basis and aggregated to annual values. We selected 26 stations with continuous records and no data gaps during the 2001–2011 period. Observed suspended sediment data were used due to both data availability and the nature of sediment transport in the region. The Loess Plateau is predominantly composed of loess soils, which are fine-grained and highly erodible. Previous studies have shown that bedload accounts for only 2%–7% of the total sediment load in this region (Huang et al. 2007).

The Nash–Sutcliffe model efficiency and determination coefficients (R^2) were employed to evaluate the performance of the simulation results.

2.6 | Data Acquisition

Monthly precipitation data from 28 meteorological stations within and around the study area of 2001–2011 were obtained from the National Meteorological Information Centre to calculate the rainfall erosivity factor (Equation 5b) for both the RUSLE and AIC. The rainfall map was generated using Spline interpolation (suitable for large scale mapping; (Angulo-Martínez and Beguería 2009)), and in the AIC calculation the value range was normalized between 0.001 and 1.

To estimate the *C* factor in RUSLE, IC and AIC, yearly ground cover maps for the region of year 2001–2011 were provided by Yang et al. (2020). Sand (%), silt (%), clay (%), and the total organic carbon (%) content of the soil for the *K* factor calculation in the RUSLE equation for the period 2001–2011 and soil available water content (m^3/m^3) to calculate the K_p factor in the AIC were obtained from HiHydroSoil v1.2 (De Boer 2016). The soil permeability factor (K_p) map used in the AIC calculation was calculated from the normalized and inverse value of soil available water content (Wu et al. 2023).

To calculate the LS and *P* factors in the RUSLE equation and *S* and RT factors in the IC and the AIC, a 30 × 30 m resolution DEM was obtained from Geospatial Data Cloud (http://www.gscloud.cn/) freely. To ensure overland flow continuity, local sinks were removed using the fill tool in ArcGIS Pro 2.4.3.

3 | Results

3.1 | Sediment Yield Predictions With InVEST-SDR$_{IC}$ and InVEST-SDR$_{AIC}$

The relation between observed sediment yield (SYobs; t year^{-1}) and (a) catchment area, (b) RUSLE estimated soil erosion, and estimated sediment yield (SYest; t year^{-1}) calculated using (c) IC and (d) AIC, respectively, is shown in Figure 2. As expected, the values of SYobs in the 26 sub-catchments (mean ($\bar{x}$) = 1.95E+07; median ($\tilde{x}$) = 6.98E+06; standard deviation (σ) = 3.11E+07 t year^{-1}) showed a strong positive linear correlation with the sub-catchment size ($\bar{x}$ = 8.61E+05; $\tilde{x}$ = 3.29E+05; σ = 1.15E+06 ha), with R^2 = 0.76 (Figure 2a). The RUSLE-calculated soil erosion ($\bar{x}$ = 2.96E+07; $\tilde{x}$ = 1.26E+07; σ = 4.09E+07 t year^{-1}) showed a better correlation with observed SY with R^2 = 0.89 (Figure 2b), obtaining acceptable simulation results –the Nash-Sutcliffe Efficiency was equal to 0.65. The use of the two connectivity approaches improved the regression between SYobs and SYest: R^2 = 0.932 for SYest-IC ($\bar{x}$ = 7.56E+06; $\tilde{x}$ = 2.89E+06; σ = 1.06E+07 t year^{-1}) and R^2 = 0.9102 (Figure 2c) for SYest-AIC ($\bar{x}$ = 6.11E+06; $\tilde{x}$ = 2.41E+06; σ = 8.52E+06 t year^{-1}) (Figure 2d). The Nash-Sutcliffe Efficiency between SYobs and SYest-IC was −0.41, while for SYobs and SYest-AIC it was 0.47. These results suggest that the sediment yield estimated using the AIC-based approach provides a more satisfactory prediction.

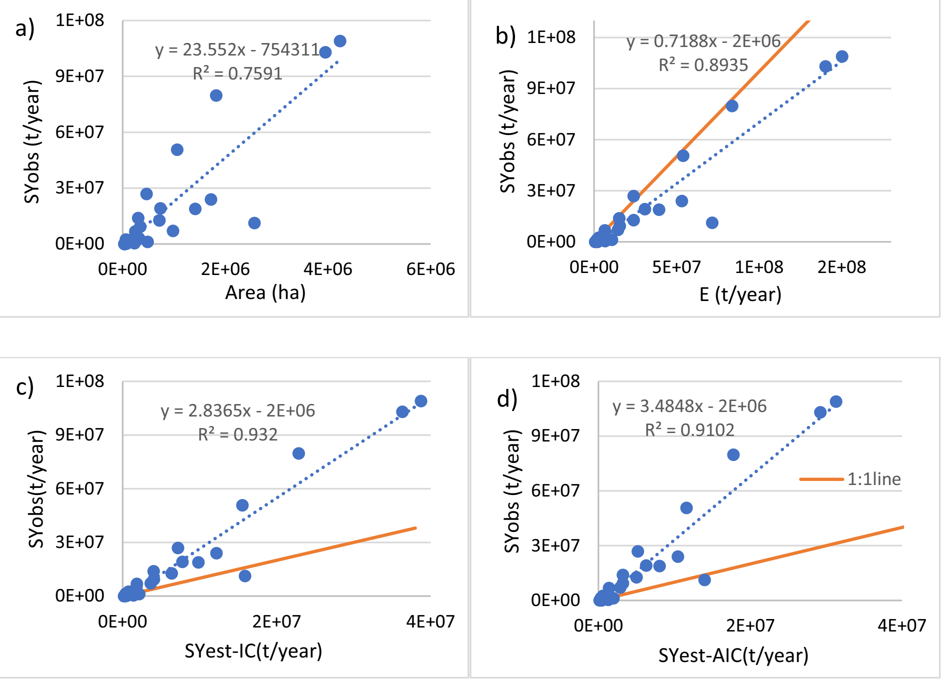

FIGURE 2 | Relations between observed sediment yield (SYobs) and (a) catchment area, (b) RUSLE-estimated soil erosion, and estimated sediment yield (SYest) calculated with InVEST-SDR$_{IC}$ (c) and InVEST-SDR$_{AIC}$ (d). [Colour figure can be viewed at wileyonlinelibrary.com]

3.2 | Spatial Variation of AIC in the Different Sub-Catchments

In Figure 3a, the 26 sub-catchments (stations at their outlet) were ranked according to their size. For each catchment, the column indicates the proportion of the 90th percentile (P90 in red; high connectivity values) and the 10th percentile (P10 in green; low connectivity values) within the catchment. In general, a positive relationship between observed SY and sub-catchment size (Figure 3a) was found. It is also clear that catchments with a higher percentage of P90 values, have a higher SY. It should be noted that 54% of the P90 values were found in the three sub-catchments with the highest observed SY (catchments Jingcun (k), Zhangjiashan (l) and Yuluoping (q)). However, when the values of observed SY were expressed per unit area (SSY: specific sediment yield), we found that the highest values of SSY appeared concentrated in a specific zone. Figure 3b plots SSY for catchments ranked according to their closeness to the basin outlet (Fenglingdu). As can be seen, catchments Gangu (a), Hongde (o), Qingyang (p), Yuluoping (q), Jiaqiao (r) and Yuele (s) that are located relatively far from the main basin outlet, had the highest SSY. These stations are located, on average, at 295 km from the outlet and together contain 31% of all P90 connectivity values. (Figure 3b). These results shed light on the identification of those sub-catchments with the most intense soil erosion, which are not located near the outlet of the Wei River Basin. In addition, these erosion-prone sub-catchments also presented the highest percentages of areas with high sediment connectivity (Figure 3b).

3.3 | Temporal and Spatial Patterns of AIC

Among the five factors of AIC, only the *R* factor showed a consistent temporal trend with the 90th percentile of functional connectivity as shown in Figure 4. For example, high values of both AIC and *R* occurred in 2003 and low values in 2008–2009. Spatially, the consistency was not obvious (Figure 5a,b): the northwest of the basin was relatively dry during the study period, while the southeast area was wet (Figure 5b). Low connectivity areas (P10, green colors) were generally located in the plain area in the Wei sub-basin, in the table land in the Beiluo sub-basin and in the central part of the Jing sub-basin (Figure 5a). In 2001, 2002, 2007 and 2011, high connectivity (P90, red colors) was concentrated in the north part of the Jing sub-basin; in 2004, 2005 and 2009, high connectivity areas moved to the east part of the Wei sub-basin and north part of the Jing sub-basin; and in 2003, 2006, 2008 and 2010, high connectivity covered the Jing sub-catchment and the east part of the Wei sub-catchment. The spatial inconsistency observed between the *R*-factor distribution and the high and low AIC values suggests that functional components, such as rainfall erosivity, may not be the dominant drivers of sediment connectivity in the headwater regions. This indicates that structural factors likely play a more significant role in governing sediment transport processes in these areas.

3.4 | Functional Versus Structural Connectivity

We calculated the correlation between 11 AIC maps and 11 *R*-factor maps, as well as 11 AIC maps and 11 *C*-factor maps,

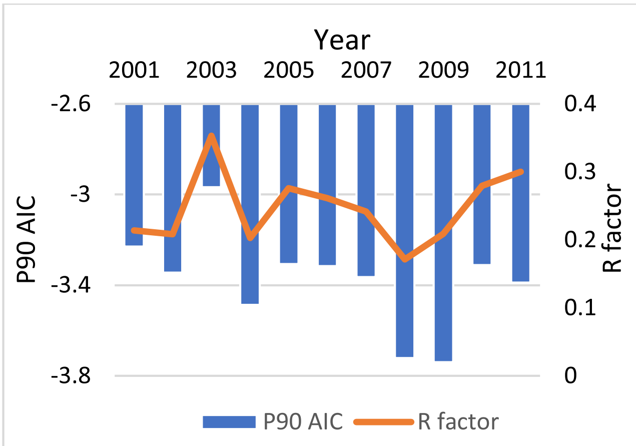

FIGURE 4 | 90th percentile of AIC and *R* factor for the Wei River Basin during years 2001 and 2011. [Colour figure can be viewed at wileyonlinelibrary.com]

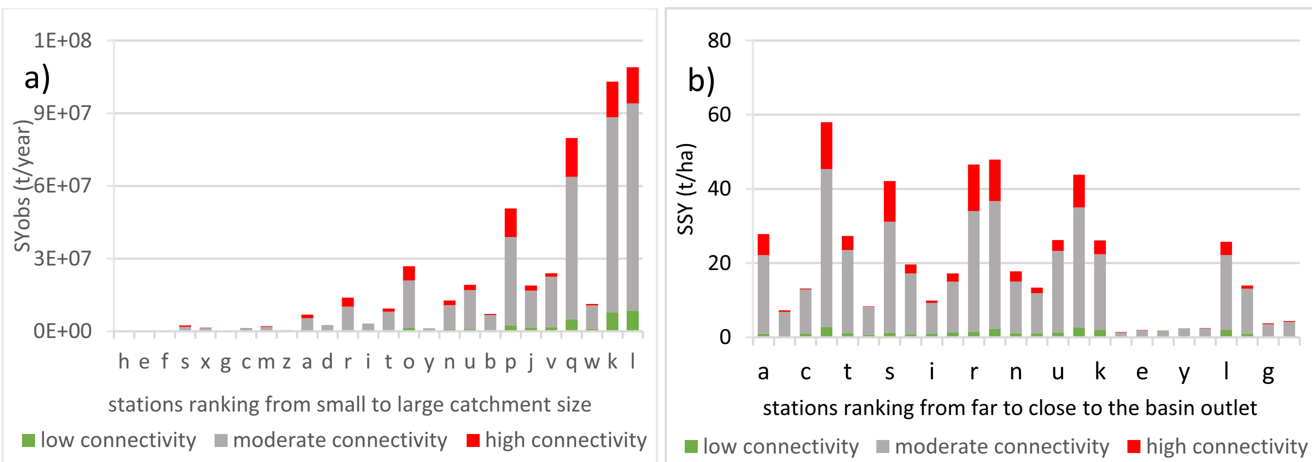

FIGURE 3 | Proportion of percentile 90% (P90) and 10% (P10) of sediment connectivity (AIC) of the 26 sub-catchments plotted against (a) observed sediment yield and (b) specific sediment yield. In (a) the sub-catchment stations are ranked by their catchment size; in (b) they were ranked according to their closeness to the outlet of the entire basin. The letters shown on the x-axis correspond to the hydrometric stations presented in Figure 1. [Colour figure can be viewed at wileyonlinelibrary.com]

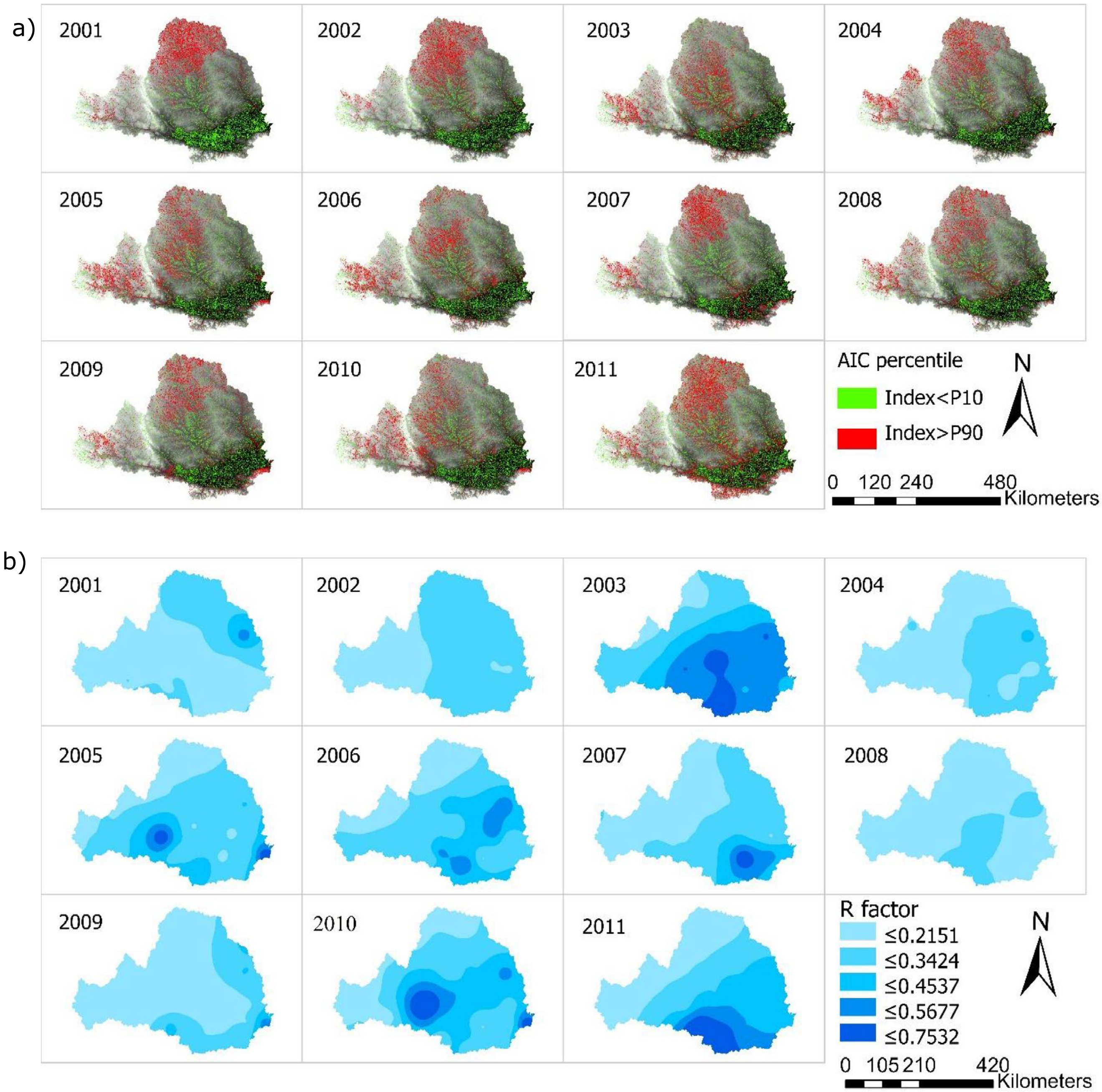

FIGURE 5 | (a) AIC maps with highest (P90) and lowest (P10) percentiles of AIC values and (b) Rainfall erosivity maps for years 2001–2011. [Colour figure can be viewed at wileyonlinelibrary.com]

corresponding to the observation years. A correlation coefficient greater than 0.682 was considered statistically significant ($p<0.01$). The results of the significance of the correlation between AIC and the *R* factor, as well as AIC and the *C* factor, are presented in two maps in Figure 6. Figure 6a shows that the *R* factor was significantly and positively correlated with AIC across almost the entire study area (depicted in green). In contrast, Figure 6b indicates that the *C* factor exhibited a positive correlation with AIC in most parts of the basin (green and dark orange), but only a few areas demonstrated a statistically significant relationship (in green, $p<0.01$). Additionally, an insignificant negative correlation (depicted in light orange) was observed in the mountainous regions of the basin. This suggests that, in these mountainous areas, the *C* factor was not the dominant determinant of AIC.

To better understand the temporal and spatial variation of AIC, and the dominant regions of structural or functional connectivity, we compared AIC and IC (Figure 7). The differences in P90 values between AIC and IC occurred mainly in three regions. In the western part of the basin where the altitude is relatively high (Figure 7b,f), and the K_p factor is relatively high (Figure 7i). Here, K_p reduced the connectivity (AIC vs. IC): where the K_p factor values were high (indicating low soil available water content and therefore greater potential for rainfall storage in the soil), P90 values of AIC occurred less

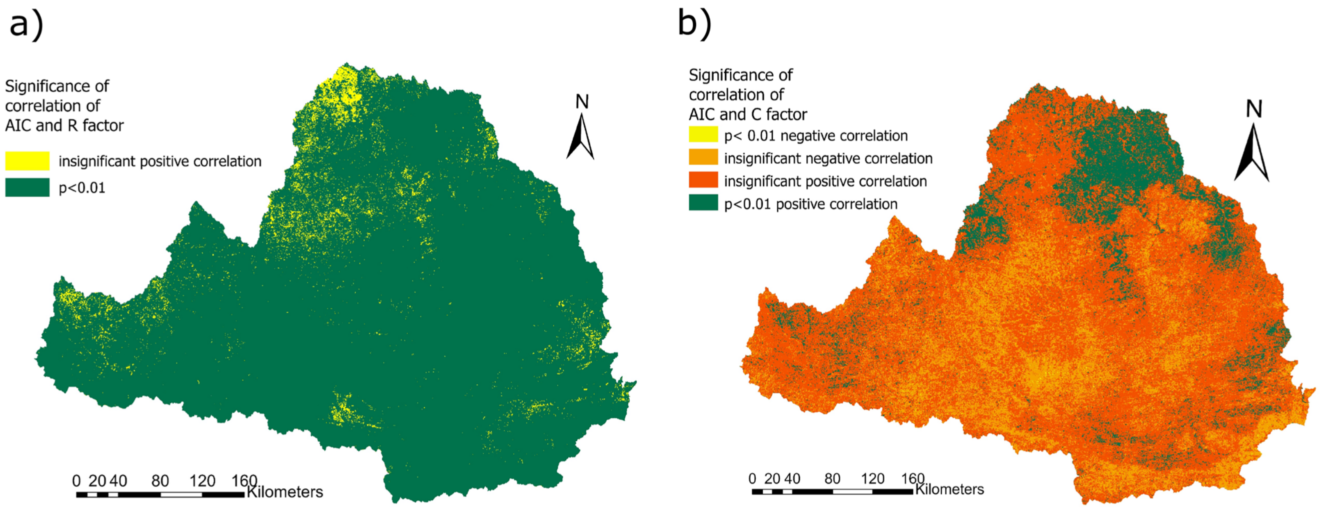

FIGURE 6 | Maps of significance of correlation of AIC and (a) *R* factor and (b) *C* factor. [Colour figure can be viewed at wileyonlinelibrary.com]

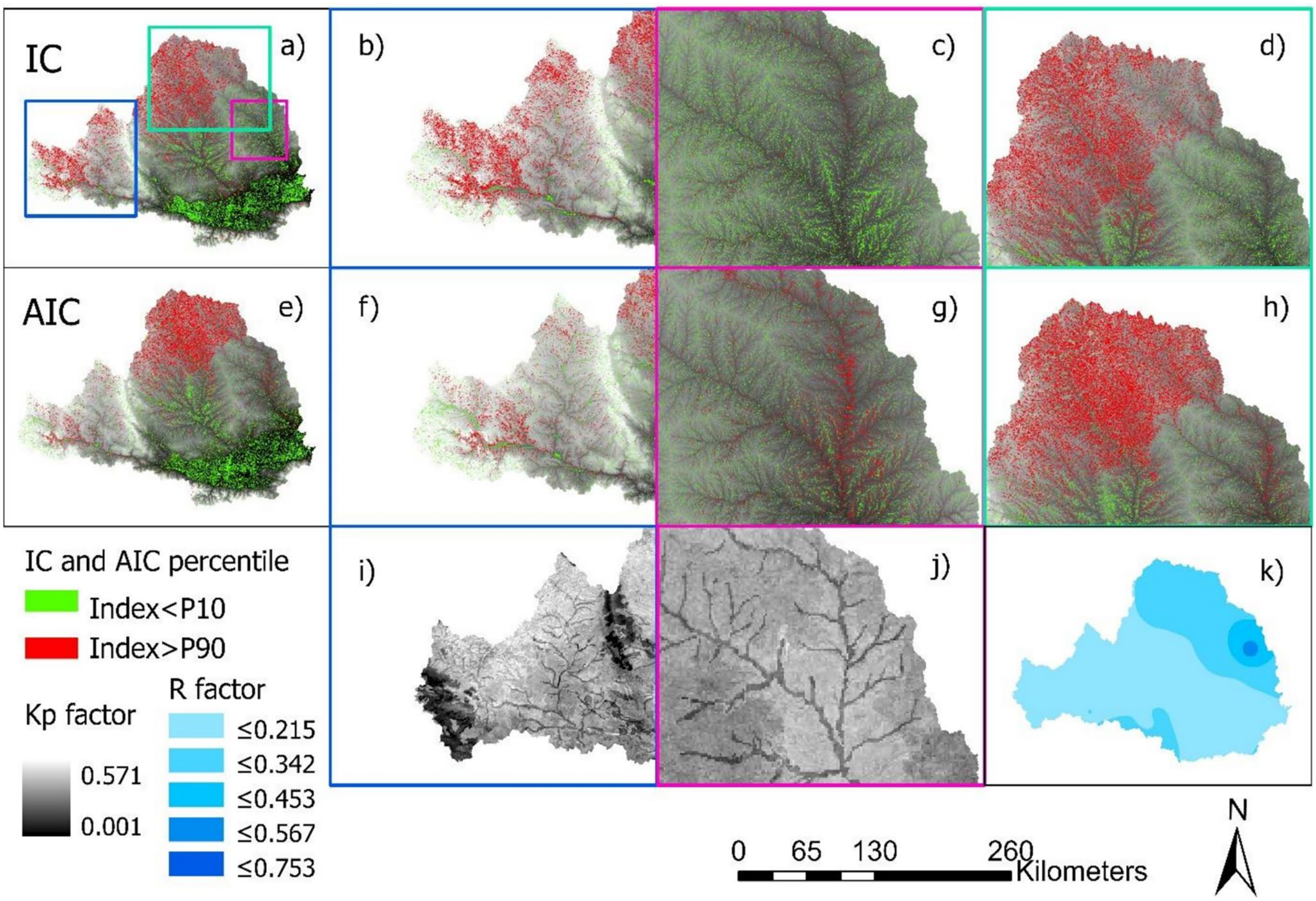

FIGURE 7 | Maps of IC (a) and AIC (e) of year 2001 and detailed maps of IC and AIC in (b, f) the west part of the basin, (c, g) river channel of the east part of the basin, (d, h) the north part of the basin, detailed maps of the K_p factor (i) and (j) in the corresponding area and the *R* factor map of the whole basin (k). [Colour figure can be viewed at wileyonlinelibrary.com]

frequently than P90 values of IC. In the northern part of the basin, where the *R* factor is high (Figure 7k), the AIC P90 values were more widespread (Figure 7h) as compared to the IC P90 values (Figure 7d). In the river channel in the eastern part of the basin where the K_p factor is relatively low (i.e., higher soil available water content in the channels; Figure 7j), the P90 values of AIC were more concentrated (Figure 7g) than the P90 values of the IC (Figure 7c).

4 | Discussion

4.1 | Prediction Ability of InVEST-SDR$_{IC}$ and InVEST-SDR$_{AIC}$

In the last decade, several studies have applied and proved InVEST-SDR to be useful for estimating sediment export at the catchment scales of semiarid erosion-prone areas (Bouguerra and Jebari 2017; Hamel et al. 2017; Marques et al. 2021; Zhao et al. 2020). For instance, Marques et al. (2021) quantified the effects of land use changes on sediment retention in mainland Portugal; Bouguerra and Jebari (2017) calculated sediment loss in the Rmel river basin in Tunisia and proved the utility of the InVEST-SDR model in identifying the priority zones for soil and water conservation. In this study, we aimed to verify the sediment connectivity results calculated from AIC, instead of the standard IC, using the InVEST-SDR model and observed sediment yield data. Our results showed that both IC and AIC performed well in terms of predicting sediment yield at the large basin scale (Figure 2). However, the estimated sediment yield was lower than the observed sediment yield. Two possible reasons may explain this discrepancy. First, the simplification of the processes included in the InVEST-SDR model, since the model predicts only interrill erosion (through RUSLE calculations), additional sediment sources such as bank erosion, gullies, landslides, or legacy sediments are not considered by the model (Hamel et al. 2017). Second, the estimated soil erosion rate in this study was possibly low. Several studies have estimated soil erosion rates for the Loess Plateau using the RUSLE equation; the results differ from a range of 500–4000 $t{\cdot}km^{-2}{\cdot}a^{-1}$. Jin et al. (2021) reported 595 $t{\cdot}km^{-2}{\cdot}a^{-1}$ in 2011–2015, Wen et al. (2023) estimated an annual erosion rate for the Beiluo River Catchment (a sub-catchment of the Wei River Basin) of 733.47 $t{\cdot}km^{-2}$ in 2010. Fu et al. (2011) estimated an average soil erosion rate for the Loess Plateau using the RUSLE equation of 2405 $t{\cdot}km^{-2}{\cdot}a^{-1}$ in 2008; Li, Guan, et al. (2022) estimated less than 4000 $t{\cdot}km^{-2}{\cdot}a^{-1}$ in the 2000s. Whereas in our study the RUSLE estimated erosion rate was 1743.0 $t\,km^{-2}\,a^{-1}$ in 2008, 2803.8 $t\,km^{-2}\,a^{-1}$ in 2010, and 2656.7 $t\,km^{-2}\,a^{-1}$ in the 2000s. Our estimated erosion rates fall within the range reported by other studies; however, they may still underestimate actual sediment fluxes.

Zhao et al. (2016) examined the spatiotemporal variation of sediment yield from 1957 to 2012 on the Loess Plateau and found that in the period 2000–2012 the sediment load was extremely low compared to the earlier decades. López-Vicente et al. (2017) simulated hydrological connectivity of the Japanese forest after different forest management operations, and found that progressive vegetation recovery triggered a slight reduction of connectivity. Theoretically the large scale of the vegetation recovery project in the Loess Plateau would reduce the connectivity in the study area. We studied the sediment connectivity for the time period 2001–2011, but did not find a significant decreasing trend within these 11 years. Zhang et al. (2021) estimated the area of potential risks of soil erosion caused by high rainfall erosivity in the Wei River Basin. They identified a high-risk area located in the northern part of the basin, which overlaps with our identified high-connectivity zone.

We also investigated whether structural or functional connectivity was dominant in different topographies across the basin (Figure 7) by comparing the results of IC and AIC. IC was used to map structural connectivity with average *C*-factor values (without annual changes), and AIC computed functional connectivity as it included a dynamic component: the rainfall factor with annual differences. Our findings of high values of IC prevailing in the high-altitude mountain areas in the western part of the basin, and high values of AIC synchronized with high rainfall and the river channel, align with Mahoney et al. (2021) who found that structural connectivity dominates in steep basins with high runoff, while functional connectivity controls flat basins with low hydrologic events. The investigation of structural and functional connectivity-prone areas is valuable because even though structural connectivity may be relatively stable, the basin area functionally connected in terms of sediment transport to the catchment outlet may increase up to six times during rainstorms, compared to average rainfall conditions (Buter et al. 2022). González-Romero et al. (2022) proved that the application of functional connectivity enabled the evaluation of the potential vulnerability of the system, such as in forest fire-affected areas where structural connectivity can be altered.

4.2 | Limitations and Future Research

Batista et al. (2019) pointed out that due to the uncertainty of environmental models, they cannot be truly verified or validated, but purpose-oriented critical model evaluation can lead to improvements. This study carried out an outlet-based verification, based on nested catchments. Even though the results showed a good correlation between SYest-AIC and observed sediment yield, we cannot verify if the spatial pattern is also correct as spatially explicit observations of erosion, transport and deposition are lacking.

The effect of the spatial resolution of the inputs (30 × 30 m in this study) must also be taken into account, since coarse resolutions provide average values, potentially eliminating information on soil erosion and sediment connectivity from small areas of bare soil and/or with high or very low slopes (López-Vicente and Álvarez 2018). Especially, the role of forest roads and bare soil trails in agricultural areas is not included in coarse resolutions, despite the fact that both elements act as sediment source areas and preferential export channels (Salesa and Cerdà 2020; Ramos Scharrón et al. 2023).

The K_p factor, used to calculate AIC, was evaluated from soil available water content. Additionally, other soil properties that may influence computed connectivity patterns, such as soil depth and bulk density, should be integrated into the K_p factor in future research (Zingaro et al. 2019).

5 | Conclusions

The InVEST-SDR model was applied to verify the sediment connectivity results calculated using the AIC in a large basin with many spatial heterogeneities. Results showed good performance of the model on predicting the spatial and temporal variability of sediment connectivity and sediment yield. High connectivity areas also effectively present erosion-prone catchments in the basin, and AIC appeared to be a good approach to be used for local managers as an erosion hotspot detection tool. The variation of P90 values of AIC did not show a clear trend for the period 2001–2011, but it had a consistent temporal trend with the *R* factor. The *C* factor showed insignificant negative correlation with AIC in the mountain areas in the Wei River Basin, denoting that land cover was not the determinant factor of AIC in the mountain areas. The IC and AIC maps of the year 2001 were compared to identify the dominant areas of structural or functional connectivity, and the main differences were found in three regions; structural connectivity dominated in the mountainous areas in the Wei sub-catchment compared to functional connectivity, because the K_p (soil permeability) factor of AIC was high in this region, while functional connectivity dominated in the river channel in the Beiluo sub-catchment and in the north part of the whole basin, because of the influence of the K_p and R factors of AIC, respectively. This study for the first time incorporated functional connectivity (through the AIC) in the assessment of sediment yield through the InVEST-SDR approach and applied the approach at the large basin scale, where detailed data is unavailable to apply, for example, detailed process-based erosion models.

Acknowledgements

The China Scholarship Council funded this work through the grant attributed to Z. Wu (CSC: 201906300050). The authors would like to acknowledge Prof. Xihua Yang for providing his research findings and data for the C-RUSLE factor preparation in this study.

Funding

This work was supported by China Scholarship Council.

Data Availability Statement

The data that support the findings of this study are available from the corresponding author upon reasonable request.

References

Abebe, N., J. Eekhout, B. Vermeulen, et al. 2023. "The Potential and Challenges of the 'RUSLE-IC-SDR' Approach to Identify Sediment Dynamics in a Mediterranean Catchment." *Catena* 233: 107480. https://doi.org/10.1016/j.catena.2023.107480.

Angulo-Martínez, M., and S. Beguería. 2009. "Estimating Rainfall Erosivity From Daily Precipitation Records: A Comparison Among Methods Using Data From the Ebro Basin (NE Spain)." *Journal of Hydrology* 379, no. 1–2: 111–121. https://doi.org/10.1016/j.jhydrol.2009.09.051.

Batista, P. V. G., J. Davies, M. L. N. Silva, and J. N. Quinton. 2019. "On the Evaluation of Soil Erosion Models: Are We Doing Enough?" *Earth-Science Reviews* 197: 102898. https://doi.org/10.1016/j.earscirev.2019.102898.

Bhattacharya, R. K., N. Das Chatterjee, and K. Das. 2024. "Modelling of Soil Erosion Susceptibility Incorporating Sediment Connectivity and Export at Landscape Scale Using Integrated Machine Learning, InVEST-SDR and Fragstats." *Journal of Environmental Management* 353: 120164. https://doi.org/10.1016/j.jenvman.2024.120164.

Bombino, G., C. Boix-Fayos, M. F. Cataldo, et al. 2020. "A Modified Catchment Connectivity Index for Applications in Semi-Arid Torrents of the Mediterranean Environment." *River Research and Applications* 36, no. 5: 735–748. https://doi.org/10.1002/rra.3606.

Borrelli, P., D. A. Robinson, L. R. Fleischer, et al. 2017. "An Assessment of the Global Impact of 21st Century Land Use Change on Soil Erosion." *Nature Communications* 8, no. 1: 2013. https://doi.org/10.1038/s41467-017-02142-7.

Borselli, L., P. Cassi, and D. Torri. 2008. "Prolegomena to Sediment and Flow Connectivity in the Landscape: A GIS and Field Numerical Assessment." *Catena* 75, no. 3: 268–277. https://doi.org/10.1016/j.catena.2008.07.006.

Bouguerra, S., and S. Jebari. 2017. "Identification and Prioritization of Sub-Watersheds for Land and Water Management Using InVEST SDR Model: Rmelriver Basin, Tunisia." *Arabian Journal of Geosciences* 10, no. 15: 348. https://doi.org/10.1007/s12517-017-3104-z.

Bracken, L. J., L. Turnbull, J. Wainwright, and P. Bogaart. 2015. "Sediment Connectivity: A Framework for Understanding Sediment Transfer at Multiple Scales." *Earth Surface Processes and Landforms* 40, no. 2: 177–188. https://doi.org/10.1002/esp.3635.

Buter, A., T. Heckmann, L. Filisetti, et al. 2022. "Effects of Catchment Characteristics and Hydro-Meteorological Scenarios on Sediment Connectivity in Glacierised Catchments." *Geomorphology* 402: 108128. https://doi.org/10.1016/j.geomorph.2022.108128.

Cavalli, M., S. Trevisani, F. Comiti, and L. Marchi. 2013. "Geomorphometric Assessment of Spatial Sediment Connectivity in Small Alpine Catchments." *Geomorphology* 188: 31–41. https://doi.org/10.1016/j.geomorph.2012.05.007.

Cislaghi, A., and G. B. Bischetti. 2019. "Source Areas, Connectivity, and Delivery Rate of Sediments in Mountainous-Forested Hillslopes: A Probabilistic Approach." *Science of the Total Environment* 652: 1168–1186. https://doi.org/10.1016/j.scitotenv.2018.10.318.

Crema, S., and M. Cavalli. 2018. "SedInConnect: A Stand-Alone, Free and Open Source Tool for the Assessment of Sediment Connectivity." *Computers & Geosciences* 111: 39–45. https://doi.org/10.1016/j.cageo.2017.10.009.

De Boer, F. 2016. *HiHydroSoil: A High Resolution Soil Map of Hydraulic Properties. Version 1.2*. Futurewater. https://www.futurewater.nl/wp-content/uploads/2015/05/HiHydroSoil-A-high-resolution-soil-map-of-hydraulic-properties.pdf.

de Vente, J., J. Poesen, M. Arabkhedri, and G. Verstraeten. 2016. "The Sediment Delivery Problem Revisited." *Progress in Physical Geography: Earth and Environment* 31, no. 2: 155–178. https://doi.org/10.1177/0309133307076485.

de Vente, J., J. Poesen, G. Verstraeten, et al. 2013. "Predicting Soil Erosion and Sediment Yield at Regional Scales: Where Do We Stand?" *Earth-Science Reviews* 127: 16–29. https://doi.org/10.1016/j.earscirev.2013.08.014.

Delmas, M., O. Cerdan, J.-M. Mouchel, and M. Garcin. 2009. "A Method for Developing a Large-Scale Sediment Yield Index for European River Basins." *Journal of Soils and Sediments* 9, no. 6: 613–626. https://doi.org/10.1007/s11368-009-0126-5.

Didoné, E. J., J. P. G. Minella, and O. Evrard. 2017. "Measuring and Modelling Soil Erosion and Sediment Yields in a Large Cultivated Catchment Under No-Till of Southern Brazil." *Soil and Tillage Research* 174: 24–33. https://doi.org/10.1016/j.still.2017.05.011.

Fu, B., Y. Liu, Y. Lü, C. He, Y. Zeng, and B. Wu. 2011. "Assessing the Soil Erosion Control Service of Ecosystems Change in the Loess Plateau of China." *Ecological Complexity* 8, no. 4: 284–293. https://doi.org/10.1016/j.ecocom.2011.07.003.

Gashaw, T., A. Bantider, G. Zeleke, et al. 2021. "Evaluating InVEST Model for Estimating Soil Loss and Sediment Export in Data Scarce Regions of the Abbay (Upper Blue Nile) Basin: Implications for Land Managers." *Environmental Challenges* 5: 100381. https://doi.org/10.1016/j.envc.2021.100381.

González-Romero, J., M. López-Vicente, E. Gómez-Sánchez, et al. 2022. "Post-Fire Management Effects on Hillslope-Stream Sediment Connectivity in a Mediterranean Forest Ecosystem." *Journal of Environmental Management* 316: 115212. https://doi.org/10.1016/j.jenvman.2022.115212.

Hamel, P., R. Chaplin-Kramer, S. Sim, and C. Mueller. 2015. "A New Approach to Modeling the Sediment Retention Service (InVEST 3.0): Case Study of the Cape Fear Catchment, North Carolina, USA." *Science of the Total Environment* 524-525: 166–177. https://doi.org/10.1016/j.scitotenv.2015.04.027.

Hamel, P., K. Falinski, R. Sharp, D. A. Auerbach, M. Sanchez-Canales, and P. J. Dennedy-Frank. 2017. "Sediment Delivery Modeling in Practice: Comparing the Effects of Watershed Characteristics and Data Resolution Across Hydroclimatic Regions." *Science of the Total Environment* 580: 1381–1388. https://doi.org/10.1016/j.scitotenv.2016.12.103.

Hooke, J., and J. Souza. 2021. "Challenges of Mapping, Modelling and Quantifying Sediment Connectivity." *Earth-Science Reviews* 223: 103847. https://doi.org/10.1016/j.earscirev.2021.103847.

Huang, M., J. Gallichand, and P. Zhang. 2007. "Runoff and Sediment Responses to Conservation Practices: Loess Plateau of China1." *JAWRA Journal of the American Water Resources Association* 39, no. 5: 1197–1207. https://doi.org/10.1111/j.1752-1688.2003.tb03702.x.

Jin, F., W. Yang, J. Fu, and Z. Li. 2021. "Effects of Vegetation and Climate on the Changes of Soil Erosion in the Loess Plateau of China." *Science of the Total Environment* 773: 145514. https://doi.org/10.1016/j.scitotenv.2021.145514.

Li, H., Q. Guan, Y. Sun, et al. 2022. "Spatiotemporal Analysis of the Quantitative Attribution of Soil Water Erosion in the Upper Reaches of the Yellow River Basin Based on the RUSLE-TLSD Model." *Catena* 212: 106081. https://doi.org/10.1016/j.catena.2022.106081.

Li, P., J. Chen, G. Zhao, et al. 2022. "Determining the Drivers and Rates of Soil Erosion on the Loess Plateau Since 1901." *Science of the Total Environment* 823: 153674. https://doi.org/10.1016/j.scitotenv.2022.153674.

Liu, B. Y., M. A. Nearing, and L. M. Risse. 1994. "Slope Gradient Effects on Soil Loss for Steep Slopes." *Transactions of ASAE* 37, no. 6: 1835–1840. https://doi.org/10.13031/2013.28273.

Liu, K., J. Na, C. Fan, et al. 2022. "Large-Scale Detection of the Tableland Areas and Erosion-Vulnerable Hotspots on the Chinese Loess Plateau." *Remote Sensing* 14, no. 8: 1946. https://doi.org/10.3390/rs14081946.

Llena, M., D. Vericat, M. Cavalli, S. Crema, and M. W. Smith. 2019. "The Effects of Land Use and Topographic Changes on Sediment Connectivity in Mountain Catchments." *Science of the Total Environment* 660: 899–912. https://doi.org/10.1016/j.scitotenv.2018.12.479.

López-Vicente, M., and S. Álvarez. 2018. "Influence of DEM Resolution on Modelling Hydrological Connectivity in a Complex Agricultural Catchment With Woody Crops." *Earth Surface Processes and Landforms* 43, no. 7: 1403–1415. https://doi.org/10.1002/esp.4321.

López-Vicente, M., and N. Ben-Salem. 2019. "Computing Structural and Functional Flow and Sediment Connectivity With a New Aggregated Index: A Case Study in a Large Mediterranean Catchment." *Science of the Total Environment* 651, no. Pt 1: 179–191. https://doi.org/10.1016/j.scitotenv.2018.09.170.

López-Vicente, M., J. Poesen, A. Navas, and L. Gaspar. 2013. "Predicting Runoff and Sediment Connectivity and Soil Erosion by Water for Different Land Use Scenarios in the Spanish Pre-Pyrenees." *CATENA* 102: 62–73. https://doi.org/10.1016/j.catena.2011.01.001.

López-Vicente, M., X. Sun, Y. Onda, H. Kato, T. Gomi, and M. Hiraoka. 2017. "Effect of Tree Thinning and Skidding Trails on Hydrological Connectivity in Two Japanese Forest Catchments." *Geomorphology* 292: 104–114. https://doi.org/10.1016/j.geomorph.2017.05.006.

Lu, H., C. J. Moran, and I. P. Prosser. 2006. "Modelling Sediment Delivery Ratio Over the Murray Darling Basin." *Environmental Modelling and Software* 21, no. 9: 1297–1308. https://doi.org/10.1016/j.envsoft.2005.04.021.

Lufafa, A., M. M. Tenywa, M. Isabirye, M. J. G. Majaliwa, and P. L. Woomer. 2003. "Prediction of Soil Erosion in a Lake Victoria Basin Catchment Using a GIS-Based Universal Soil Loss Model." *Agricultural Systems* 76, no. 3: 883–894. https://doi.org/10.1016/s0308-521x(02)00012-4.

Mahoney, D., B. Blandford, and J. Fox. 2021. "Coupling the Probability of Connectivity and RUSLE Reveals Pathways of Sediment Transport and Soil Loss Rates for Forest and Reclaimed Mine Landscapes." *Journal of Hydrology* 594: 125963. https://doi.org/10.1016/j.jhydrol.2021.125963.

Marchi, L., F. Comiti, S. Crema, and M. Cavalli. 2019. "Channel Control Works and Sediment Connectivity in the European Alps." *Science of the Total Environment* 668: 389–399. https://doi.org/10.1016/j.scitotenv.2019.02.416.

Marques, S. M., F. S. Campos, J. David, and P. Cabral. 2021. "Modelling Sediment Retention Services and Soil Erosion Changes in Portugal: A Spatio-Temporal Approach." *ISPRS International Journal of Geo-Information* 10, no. 4: 262. https://doi.org/10.3390/ijgi10040262.

Mekonnen, M., S. D. Keesstra, J. E. M. Baartman, L. Stroosnijder, and J. Maroulis. 2016. "Reducing Sediment Connectivity Through Man-Made and Natural Sediment Sinks in the Minizr Catchment, Northwest Ethiopia." *Land Degradation & Development* 28, no. 2: 708–717. https://doi.org/10.1002/ldr.2629.

Najafi, S., D. Dragovich, T. Heckmann, and S. H. Sadeghi. 2021. "Sediment Connectivity Concepts and Approaches." *Catena* 196: 104880. https://doi.org/10.1016/j.catena.2020.104880.

Persichillo, M. G., M. Bordoni, M. Cavalli, S. Crema, and C. Meisina. 2018. "The Role of Human Activities on Sediment Connectivity of Shallow Landslides." *Catena* 160: 261–274. https://doi.org/10.1016/j.catena.2017.09.025.

Poeppl, R. E., S. D. Keesstra, and J. Maroulis. 2017. "A Conceptual Connectivity Framework for Understanding Geomorphic Change in Human-Impacted Fluvial Systems." *Geomorphology* 277: 237–250. https://doi.org/10.1016/j.geomorph.2016.07.033.

Ramos Scharrón, C. E., E. E. Alicea, Y. Figueroa Sánchez, et al. 2023. "Three Decades of Road and Trail Runoff and Erosion Work in the Northeastern Caribbean – A Research Program Perspective." *Journal of the ASABE* 66, no. 1: 35–45. https://doi.org/10.13031/ja.15078.

Salesa, D., and A. Cerdà. 2020. "Soil Erosion on Mountain Trails as a Consequence of Recreational Activities. A Comprehensive Review of the Scientific Literature." *Journal of Environmental Management* 271: 110990. https://doi.org/10.1016/j.jenvman.2020.110990.

Tangi, M., S. Bizzi, R. Schmitt, and A. Castelletti. 2023. "Balancing Sediment Connectivity and Energy Production via Optimized Reservoir Sediment Management Strategies." *Water Resources Research* 59, no. 6: e2022WR034033. https://doi.org/10.1029/2022wr034033.

Tian, P., L. Liu, X. Tian, et al. 2022. "Sediment Yields Variation and Response to the Controlling Factors in the Wei River Basin, China." *CATENA* 213: 106181. https://doi.org/10.1016/j.catena.2022.106181.

Tian, X., G. Zhao, X. Mu, et al. 2023. "Decoupling Effects of Driving Factors on Sediment Yield in the Chinese Loess Plateau." *International Soil and Water Conservation Research* 11, no. 1: 60–74. https://doi.org/10.1016/j.iswcr.2022.05.007.

Vázquez-Tarrío, D., V. Ruiz-Villanueva, J. Garrote, et al. 2024. "Effects of Sediment Transport on Flood Hazards: Lessons Learned and Remaining Challenges." *Geomorphology* 446: 108976.

Vigiak, O., L. Borselli, L. T. H. Newham, J. McInnes, and A. M. Roberts. 2012. "Comparison of Conceptual Landscape Metrics to Define Hillslope-Scale Sediment Delivery Ratio." *Geomorphology* 138, no. 1: 74–88. https://doi.org/10.1016/j.geomorph.2011.08.026.

Wen, B., C. Huang, C. Zhou, H. Zhang, Q. Yang, and M. Li. 2023. "Spatiotemporal Dynamics and Driving Factors of Soil Erosion in the Beiluo River Basin, Loess Plateau, China." *Ecological Indicators* 155: 110976. https://doi.org/10.1016/j.ecolind.2023.110976.

Wohl, E. 2015. "Legacy Effects on Sediments in River Corridors." *Earth-Science Reviews* 147: 30–53. https://doi.org/10.1016/j.earscirev.2015.05.001.

Wu, Z., J. E. M. Baartman, J. Pedro Nunes, and M. López-Vicente. 2023. "Intra-Annual Sediment Dynamic Assessment in the Wei River Basin, China, Using the AIC Functional-Structural Connectivity Index."

Ecological Indicators 146: 109775. https://doi.org/10.1016/j.ecolind.2022.109775.

Xie, Y., S.-q. Yin, B.-y. Liu, M. A. Nearing, and Y. Zhao. 2016. "Models for Estimating Daily Rainfall Erosivity in China." *Journal of Hydrology* 535: 547–558. https://doi.org/10.1016/j.jhydrol.2016.02.020.

Yang, X., X. Zhang, D. Lv, et al. 2020. "Remote Sensing Estimation of the Soil Erosion Cover-Management Factor Over China's Loess Plateau." *Land Degradation & Development* 31: 1942–1955. https://doi.org/10.1002/ldr.3577.

Zanandrea, F., G. P. Michel, M. Kobiyama, G. Censi, and B. H. Abatti. 2021. "Spatial-Temporal Assessment of Water and Sediment Connectivity Through a Modified Connectivity Index in a Subtropical Mountainous Catchment." *Catena* 204: 105380. https://doi.org/10.1016/j.catena.2021.105380.

Zhang, Y., Y. Chao, R. Fan, et al. 2021. "Spatial-Temporal Trends of Rainfall Erosivity and Its Implication for Sustainable Agriculture in the Wei River Basin of China." *Agricultural Water Management* 245: 106557. https://doi.org/10.1016/j.agwat.2020.106557.

Zhao, G., P. Gao, P. Tian, W. Sun, J. Hu, and X. Mu. 2020. "Assessing Sediment Connectivity and Soil Erosion by Water in a Representative Catchment on the Loess Plateau, China." *Catena* 185: 104284. https://doi.org/10.1016/j.catena.2019.104284.

Zhao, G., X. Mu, J. Jiao, et al. 2016. "Evidence and Causes of Spatiotemporal Changes in Runoff and Sediment Yield on the Chinese Loess Plateau." *Land Degradation & Development* 28, no. 2: 579–590. https://doi.org/10.1002/ldr.2534.

Zhao, G., X. Mu, Z. Wen, F. Wang, and P. Gao. 2013. "Soil Erosion, Conservation, and Eco-Environment Changes in the Loess Plateau of China." *Land Degradation & Development* 24, no. 5: 499–510. https://doi.org/10.1002/ldr.2246.

Zhu, Y., X. Jia, J. Qiao, and M. Shao. 2019. "What Is the Mass of Loess in the Loess Plateau of China?" *Science Bulletin* 64, no. 8: 534–539. https://doi.org/10.1016/j.scib.2019.03.021.

Zingaro, M., A. Refice, E. Giachetta, et al. 2019. "Sediment Mobility and Connectivity in a Catchment: A New Mapping Approach." *Science of the Total Environment* 672: 763–775. https://doi.org/10.1016/j.scitotenv.2019.03.461.

Supporting Information

Additional supporting information can be found online in the Supporting Information section. **Table S1:** Detail information of observed sediment yield data of 26 stations of 2001–2011.